

SiliconPV 2012

Photoluminescence imaging under applied bias for characterization of Si surface passivation layers

Halvard Haug¹, Ørnulf Nordseth¹, Edouard V. Monakhov^{2,1}, and Erik Stensrud Marstein^{1,2}

¹ Institute for Energy Technology, Instituttveien 18, 2007 Kjeller, Norway,
Phone: +47 63806233, E-mail: halvard.haug@ife.no

² Department of Physics/Center for Materials Science and Nanotechnology University of Oslo,
P.O. Box 1048 Blindern, N-0316 Oslo, Norway

Abstract

In this work, we present a novel characterization technique for the analysis of Si surface passivation layers, using a photoluminescence imaging setup. In this technique the effective lifetime of passivated Si wafers is measured while applying an external bias over a rear side dielectric film. We demonstrate that this method can be used to analyze the passivation of silicon surfaces in inversion, depletion and accumulation conditions. In this paper the method is illustrated by characterization of a-SiN_x:H passivation layers deposited by plasma enhanced chemical vapor deposition. The characterization results are interpreted both in the framework of the extended Shockley-Read Hall theory and by PC1D simulations. For the a-SiN_x:H layers, the effective surface recombination velocity parameter is found to be 5-7 times larger for electrons than for holes and the fixed insulator charge density is found to be $6.1 - 6.5 \cdot 10^{11} \text{ cm}^{-2}$ under illumination, in agreement with results from capacitance-voltage measurements.

Keywords: Photoluminescence, Imaging, Field-effect, Passivation, Silicon Nitride

1. Introduction

Electronic surface passivation is a topic of high and increasing importance for the production and development of crystalline silicon solar cells. The surface recombination velocity (SRV) of a surface is greatly influenced by the presence of charges near the surface. Such fixed charges are present in commonly used surface passivation materials like hydrogenated amorphous silicon nitride a-SiN_x:H and aluminium oxide a-AlO_x:H. During measurements, charges may also be created by the application of a voltage to a gate electrode deposited on the passivation layer. However, the presence of metallic electrodes typically complicate lifetime measurements obtained with most of the common characterization methods in that they obstruct either the optical excitation or the measurement of photoconductivity arising from excess carriers. These problems have previously been overcome e.g. by using transparent electrodes [1], or more advanced two-dimensional device structures [2], but at the cost of a higher complexity of the system.

As an alternative to the use of gate electrodes, Schöfthaler et al. [3] showed that the required charges may be deposited in a corona discharge chamber. This technique has the advantage of being non-invasive, and has among others been used by Glunz et al. [4] to investigate the SRV of the Si/SiO₂ interface as a function of surface potential. However, additional surface charge measurements with a Kelvin probe is typically required in order to obtain sufficient control of the charge density. Also, varying the charge may be time-consuming, and highly isolating passivation layers are needed to avoid stability problems.

Photoluminescence (PL) imaging is a fast and non-destructive technique for spatially resolved lifetime measurements of Si wafers [5]. In this work we present a new method, based on a small modification to a PL imaging setup, for measuring the surface recombination at Si surfaces while using an external bias to precisely control the density of charge carriers at the surface. The method will be abbreviated as PL-V

throughout this paper. In contrast to previous techniques, the measurements can be carried out on readily made samples in a fast and reversible manner. In order to demonstrate the potential of this method, we have investigated the passivation properties of a-SiN_x:H layers synthesized by plasma-enhanced chemical vapour deposition (PECVD) and interpreted these properties in terms of the fixed insulator charge density Q_f and the effective surface recombination parameters for electrons and holes.

2. Experimental procedure

Samples were made from both p-type and n-type double-side polished 100-oriented monocrystalline FZ Si wafers, with a thickness of 290 μm and doping concentrations of $N_A = 5.4 \cdot 10^{15} \text{ cm}^{-3}$ and $N_D = 1.7 \cdot 10^{15} \text{ cm}^{-3}$, respectively. The wafers received a standard RCA (1+2) clean [6] and a 30 s dip in a 5% hydrofluoric acid (HF) solution prior to PECVD processing. An Oxford Instruments PlasmaLab 133 direct plasma system with an excitation frequency of 13.56 MHz was then used to deposit a 120 nm thick a-SiN_x:H layer on the rear side of the wafers and a 40 nm thick a-Si:H layer on the front side. Note that the a-Si:H passivated front surface has a low SRV and that the wafers have a high bulk lifetime of several milliseconds, so that the rear SRV could be calculated with a small error. 7 mm \times 7 mm square metal electrodes for lifetime vs. voltage (PL-V) and 1 mm diameter circular electrodes for capacitance vs. voltage (C-V) measurements were produced on the same sample by thermal evaporation of Al through a shadow mask onto the rear side a-SiN_x:H layers. Finally, low resistivity silver paste contacts were made to the Si substrate.

A schematic overview of the measurement setup is shown in Fig. 1 (a). Steady state lifetime measurements were carried out with a LIS-R1 PL imaging setup from BT imaging with an excitation wavelength of 808 nm and a constant illumination intensity of $4.2 \cdot 10^{-2} \text{ W/cm}^2$. The PL intensity was calibrated to the effective lifetime using a quasi-steady state photoconductance (QSS-PC) measurement of a reference region without metal electrodes. An external voltage source was then connected to the sample in order to obtain lifetime images with an applied bias over the rear passivation layer. An example of a PL lifetime image measured under applied voltage is shown in Fig. 1 (b).

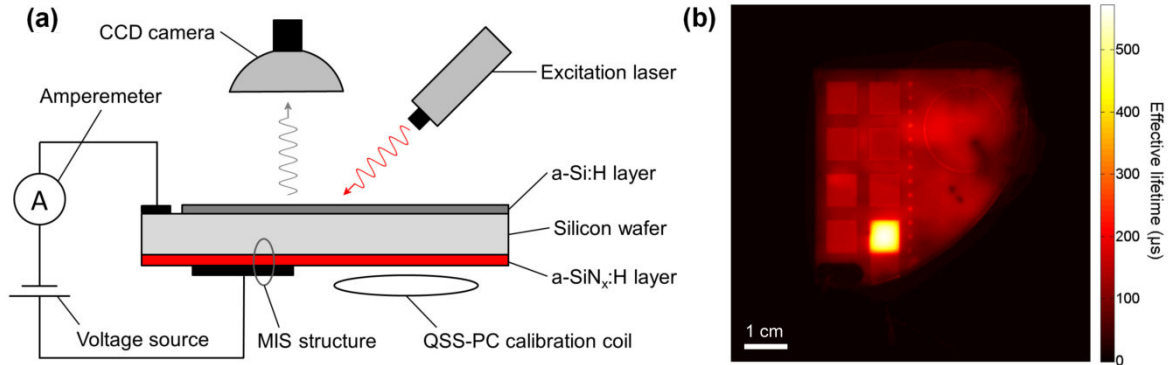


Fig. 1.

(a) Measurement setup. (b) Example of PL lifetime image measured while applying a voltage at one of the rear contacts. The locally increased effective lifetime is caused by enhanced field effect passivation.

The voltage was changed in steps of 1 V and the injection level Δn was calculated at each point from the PL intensity averaged over the central region of the contact according to the relation [7]

$$\Delta n = \sqrt{\left(\frac{N_{dop}}{2}\right)^2 + \frac{f_R \cdot I_{PL}}{C}} - \frac{N_{dop}}{2}, \quad (1)$$

where N_{dop} is the doping concentration, I_{PL} is the PL intensity and C is an instrument calibration constant which is determined from an independent quasi-steady state photoconductance (QSS-PC) measurement. f_R is

an optical correction factor that has been included to account for the fact that the addition of metal electrodes on the rear surface locally increases the rear side reflectance, causing an enhancement of the PL signal in the region above the electrodes. As the PL light may be scattered at the surfaces or reabsorbed as it passes through the wafer, this signal enhancement will depend on a number of factors, including the sample geometry, surface texturing, wafer thickness, excitation wavelength and measurement optics. The numerical value for f_R was therefore determined experimentally for each measurement. For the co-planar samples that were used in this study f_R was assumed to be given by the ratio between I_{PL} in a region placed above an electrically decoupled mirror and I_{PL} in the reference region. From these measurements f_R was found to be in the range 1.23 – 1.26 for all samples. Note that the enhanced PL signal over the metal electrodes at zero gate bias is not a good measure of the optical correction, since I_{PL} in this region is also determined by the change in the rear SRV caused by the metal-semiconductor work function difference.

The steady-state effective lifetime τ_{eff} is found from the injection level as [8]

$$\tau_{eff} = \frac{\Delta n}{G} = \frac{\Delta n}{(1 - R)\Phi_{ph}/W}, \quad (2)$$

where G is the excess carrier generation rate, Φ_{ph} is the photon flux, W is the wafer thickness and R is the reflectance, measured to be $R = 0.3$ at the excitation wavelength. Care was taken to avoid errors arising from leakage currents and changes in the insulator fixed charges during the measurements (see section 4.3 for details).

PECVD a-SiNx:H layers used for solar cell applications typically contain a high density of positive charges. The fixed insulator charge density Q_f in the a-SiNx:H layers was determined from dark C-V curves measured at a frequency of 100kHz using a Keithley 4200-SCS semiconductor characterization system. The first curve measured on each electrode, from positive to negative voltage, was used for calculating Q_f in order to reduce the error of charge buildup (hysteresis) effects on the results (see details in Sec. 3.2). Q_f is calculated from the flat band potential V_{fb} using the relation:

$$Q_f = \frac{C_i}{qA} (\phi_{ms} - V_{fb}), \quad (3)$$

where C_i is the insulator capacitance, q is the elementary charge, A is the electrode area and ϕ_{ms} is the semiconductor-metal work function difference [9] ϕ_{ms} was calculated to be $-0.84 V$ for the p-type sample and $-0.20 V$ for the n-type sample.

3. Results

3.1. Effective lifetime vs. voltage (PL-V) measurements

Fig. 2 shows the measured effective lifetime as a function of applied voltage. For increasing negative voltages ($V < 0 V$) the effective lifetime initially decreases as the external bias compensates the effect of the positive insulator charges. The effective lifetime subsequently passes through a minimum at $V_{min} \approx -5 V$, corresponding to depletion conditions at the surface, before increasing as the surface is driven into accumulation (p-type sample) or inversion (n-type sample). At large positive voltages the curve flattens out as the front side SRV starts to contribute to the effective lifetime. The effective lifetime varies between 39 and 731 μs for the p-type sample and between 101 and 1083 μs for the n-type sample. According to eq. (1) the corresponding injection level Δn also changes during the measurements, between $1.3 \cdot 10^{14}$ and $2.5 \cdot 10^{15} \text{ cm}^{-3}$ and between $3.4 \cdot 10^{14}$ and $3.7 \cdot 10^{15} \text{ cm}^{-3}$, respectively.

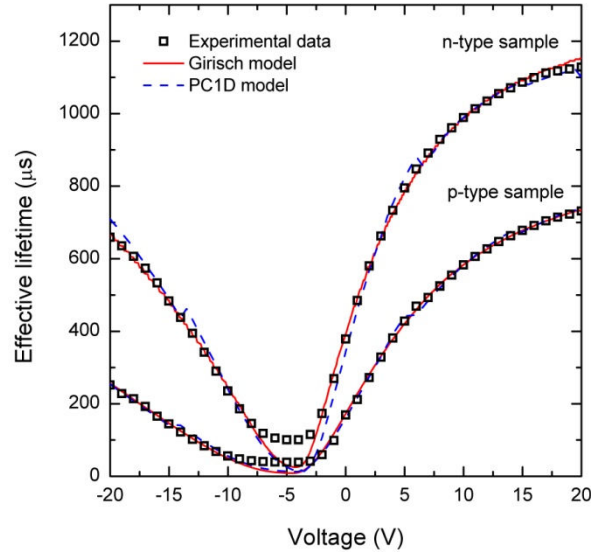


Fig. 2.

Measured (symbols) and calculated (lines) effective lifetime as a function of applied gate voltage. Simulation results from both the Girisch model and PC1D simulations (described in section 4.1 and 4.2) are shown, with the best fit parameters given in Table 2.

3.2. Capacitance-voltage measurements

A typical C-V curve measured on the n-type sample is shown in Fig. 3. The flat band voltage V_{fb} and insulator capacitance C_i were measured on 10-12 electrodes on each sample, and the corresponding fixed charge densities Q_f were calculated using eq. (3). The average values for Q_f given in Table 1 are somewhat lower than the typical values of $2-3 \cdot 10^{12} \text{ cm}^{-2}$ previously reported for PECVD a-SiN_x:H layers [10–12], but are still large enough to cause inversion conditions of the surface of the p-type samples.

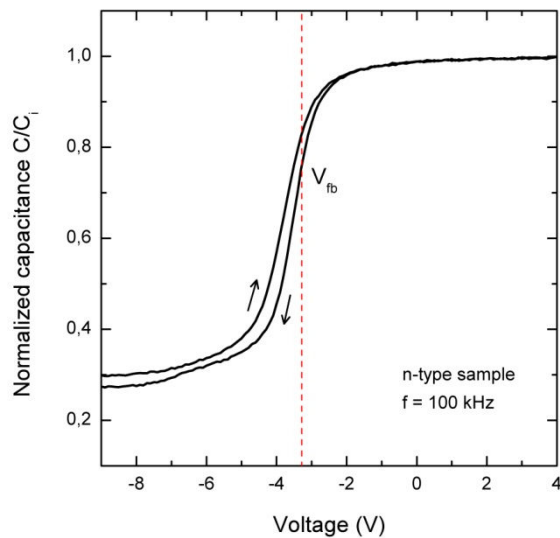


Fig. 3.

Typical capacitance vs. voltage curve measured on the n-type sample. A small hysteresis of $\sim 0.3 \text{ V}$ is observed between the initial measurement (negative sweep direction) and the reverse measurement.

	Q_f (cm^{-2})	Std. deviation (cm^{-2})
p-type sample	$7.9 \cdot 10^{11}$	$0.4 \cdot 10^{11}$
n-type sample	$7.0 \cdot 10^{11}$	$0.8 \cdot 10^{11}$

Table 1.

Fixed charge density in the a-SiN_x:H layers, determined from C-V measurements.

4. Analysis and discussion

4.1. The extended SRH formalism

In order to gain a further understanding of the surface recombination process we have calculated the rear side SRV from the extended Shockley-Read Hall (SRH) formalism described in ref. [13]. In general, the SRV of a real surface must be calculated by integration over the entire energy dependent concentration of surface states $D_{it}(E)$ [14]. However, a simplified model including one effective midgap defect level is found to sufficiently describe the observations. Moreover, it is observed that applying a different distribution of $D_{it}(E)$, for example a uniform distribution over the band gap, does not have a considerable impact on the results. The rear effective SRV is then given from standard SRH theory as:

$$S_{eff} = \frac{1}{\Delta n} \cdot \frac{n_s p_s - n_i^2}{\frac{n_s + n_i}{S_{0,p}} + \frac{p_s + n_i}{S_{0,n}}}, \quad (4)$$

where Δn is the injection level, n_i is the intrinsic carrier concentration and $S_{0,n}$ and $S_{0,p}$ are the SRV parameters of electrons and holes, defined as the product of the electron thermal velocity v_{th} , the concentration of surface state states per unit area N_{it} and the capture cross section σ_n and σ_p :

$$S_{0,n} = \sigma_n v_{th} N_{it} \quad \text{and} \quad S_{0,p} = \sigma_p v_{th} N_{it}. \quad (5)$$

In order to calculate the surface band bending and thus the surface carrier concentrations n_s and p_s arising from the applied gate voltage and the fixed insulator charges we have followed a numerical approach proposed by Girisch et al. [2]. This method is based upon balancing the charge density in the silicon Q_{Si} , the fixed charges stored in the insulating layer Q_f , the interface trapped charge Q_{it} and the charge of the gate electrode Q_g under the assumption of constant quasi Fermi levels throughout the surface space charge region. The same approach has later been used by e.g. Aberle et al. [13] and by Schmidt and Aberle [12] to calculate the SRV of Si surfaces passivated by thermal SiO₂ and a-SiN_x:H, respectively. In order to simulate the measured SRV without carrying out additional measurements for determining the properties of the surface states we have assumed that the interface trapped charge is negligible compared to the other terms, i.e. $Q_{it} = 0$. Note also that the built-in potential arising from the work function difference ϕ_{ms} between Al and Si has been implemented in the calculations. The calculated surface carrier concentrations and the surface potential ϕ_s is shown as a function of gate voltage in Fig. 4.

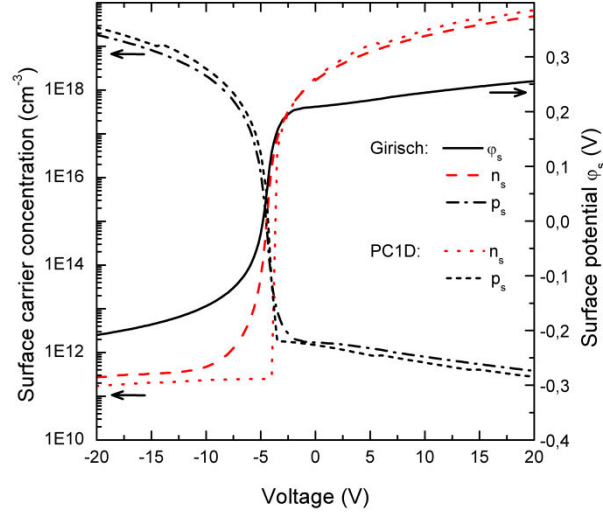


Fig. 4.

Rear side surface concentrations of electrons and holes (left axis) and surface potential ϕ_s (right axis) for the p-type sample calculated as a function of gate voltage V_g . The Girisch model and PC1D simulations that have been used for the calculations are described in section 4.1 and 4.2, respectively.

For each voltage, the excess carrier density Δn was found from the measured PL intensity and used as input to the model, and the SRV at the a-Si:H passivated front surface was calculated from eq. (4) assuming no surface band bending and $S_{0,n} = S_{0,p} = S_{0,front}$. Finally, the effective lifetime τ_{eff} was calculated from the front and rear SRVs as described in ref. [15], assuming only intrinsic contributions to the bulk lifetime. The best fit between the theoretical model and the experimental lifetime vs. voltage curve shown in Fig. 2 was then found by a multidimensional nonlinear minimization algorithm available through the Mathworks Optimization Toolbox. The rear effective SRV parameters $S_{0,n}$ and $S_{0,p}$, the front side SRV parameter $S_{0,front}$ and the fixed insulator charge density Q_f were used as free fitting parameters. The simulated curve resulting in the best fit is shown in figure 2 with the corresponding input parameters given in Table 2.

4.2. PC1D simulations

In order to demonstrate another way of interpreting the experimental results and to verify the results obtained by the Girisch model we have also simulated the measurement data using our in-house developed commando line version¹ of the PC1D software [16]. After setting up the appropriate device structure, PC1D allows all the quantities described above as input parameters with the exception of the gate voltage V_g . The effect of the gate voltage was therefore modeled as a varying effective gate charge density Q_g added to the constant fixed insulator charge Q_f , given by

$$Q_{tot} = Q_f + Q_g = Q_f + \frac{\epsilon_0 \epsilon_{SiNx}}{q d_{SiNx}} (\phi_{ms} - V_g), \quad (6)$$

where ϵ_0 is the free space permittivity, ϵ_{SiNx} is the nitride dielectric constant and d_{SiNx} is the nitride thickness. Compared to the Girisch model, this approach thus employs a similar calculation of the influence of the gate electrode, but uses a different, numerical approach to solve the coupled semiconductor equations in the Si bulk material. It also takes into account the non-uniform concentrations of charge carriers through the depth of the wafer. The steady-state effective lifetime was therefore calculated from the average excess minority concentration in the bulk, expressed by

¹ Available at http://www.ife.no/departments/solar_energy/downloads/.

$$\tau_{eff} = \frac{\int_0^W \Delta n(x) dx / W}{G}. \quad (7)$$

4.3. Simulation results

By changing V_g in steps of 0.2 V and calculating τ_{eff} at each point we could simulate the PL-V curve for any combination of $S_{0,n}$, $S_{0,p}$, $S_{0,front}$ and Q_f . As seen in Fig. 2, the theoretical models described above may be used to obtain a good fit to the experimental data. Table 2 shows that $S_{0,n}$ and $S_{0,p}$ are relatively large, suggesting that the recombination at the a-SiN_x:H/c-Si interface is mainly limited by field effect passivation. This is supported by a relatively large and positive fixed charge density, i.e. Q_f is found to be in the range $6.1 - 6.5 \cdot 10^{11} \text{ cm}^{-2}$ for both models and sample types, in good correspondence with the values obtained by C-V measurements, shown in Table 1. Note that the Q_f values determined from PL-V are measured under illumination. It has previously been suggested that Q_f in PECVD a-SiN_x:H layers are reduced by approximately one order of magnitude under illumination compared to the results of conventional dark C-V measurements [12]. Our results thus support the findings of Dauwe et al. [17], who based on measurements of the effective lifetime as a function of deposited corona charge density later reported that Q_f are in fact not changed by illumination.

Parameter	Description	Unit	P-type sample		N-type sample	
			Girisch	PC1D	Girisch	PC1D
$S_{0,n}$	SRV parameter for electrons	cm/s	$2.6 \cdot 10^5$	$3.7 \cdot 10^5$	$1.0 \cdot 10^5$	$1.6 \cdot 10^5$
$S_{0,p}$	SRV parameter for holes	cm/s	$3.7 \cdot 10^5$	$5.5 \cdot 10^4$	$2.0 \cdot 10^4$	$3.0 \cdot 10^4$
$k = S_{0,n}/S_{0,p}$	Electron hole capture ratio	-	7.0	6.7	5.1	5.3
Q_f	SiN _x fixed charge density	cm ⁻²	$6.1 \cdot 10^{11}$	$6.5 \cdot 10^{11}$	$6.4 \cdot 10^{11}$	$6.5 \cdot 10^{11}$
$S_{0,front}$	Front side SRV parameter	cm/s	38	39	31	33
N_{dop}	Doping concentration	cm ⁻³	$5.4 \cdot 10^{15}$	$5.4 \cdot 10^{15}$	$1.7 \cdot 10^{15}$	$1.7 \cdot 10^{15}$

Table 2.

Simulation parameters used as input to the extended SRH model and the PC1D simulations, giving the best fit to the results shown in Fig. 2. (Other parameters that are in common for all the simulations: $R = 0.3$, $T = 300 \text{ K}$, $W = 290 \text{ }\mu\text{m}$, $\epsilon_{SiN_x} = 3.6$, $d_{SiN_x} = 120 \text{ nm}$, $\Phi_{photon} = 1.7 \cdot 10^{17} \text{ cm}^{-2}\text{s}^{-1}$).

Another important quantity that may be determined from this analysis is the ratio between the capture cross sections of electrons and holes:

$$k = \frac{S_{0,n}}{S_{0,p}} = \frac{\sigma_n}{\sigma_p}. \quad (8)$$

The absolute values of $S_{0,n}$ and $S_{0,p}$ calculated with PC1D are $\sim 50 \%$ higher than the values found from the Girisch model. This is probably caused by a lower calculated rear surface concentration of the limiting charge carriers (see Fig. 4). The calculated k -values are however fairly consistent: as shown in Table 2, we find $k \approx 7$ for the p-type sample and $k \approx 5$ for the n-type sample regardless of the choice of model. Note also that for a known concentration of surface states N_{it} , eq. (5) may be used to independently determine the effective capture cross sections σ_n and σ_p from $S_{0,n}$ and $S_{0,p}$ in the region of the band gap most relevant for recombination.

The combination of the free parameters $S_{0,n}$, $S_{0,p}$, $S_{0,front}$ and Q_f which gives the best fit to the experimental data represent a unique solution, as the four parameters influence the calculated curve in different ways: The effect of changing Q_f is simply shifting the minimum along the voltage axis, $S_{0,front}$ causes the flattening of the curve at high lifetimes, while $S_{0,n}$ and $S_{0,p}$ determine the slope of the left-hand and right-hand part of the curve, respectively. From eq. (4) it can be seen that S_{eff} at any time is limited by the charge carrier type with the lowest surface concentration. As shown in Fig. 4, for voltages $V < V_{min}$ $n_s \gg p_s$, meaning that the last term in the denominator in eq. (4) can be omitted. S_{eff} is therefore independent of $S_{0,n}$, and the slope of this region will therefore only depend on $S_{0,p}$. Similarly, for $V > V_{min}$ the slope of S_{eff} only depends on $S_{0,n}$. Fig. 5 illustrates this point by showing the effect of varying $S_{0,n}$ while holding $S_{0,p}$ fixed (dashed red lines) and of varying $S_{0,p}$ while holding $S_{0,n}$ fixed (solid black lines).

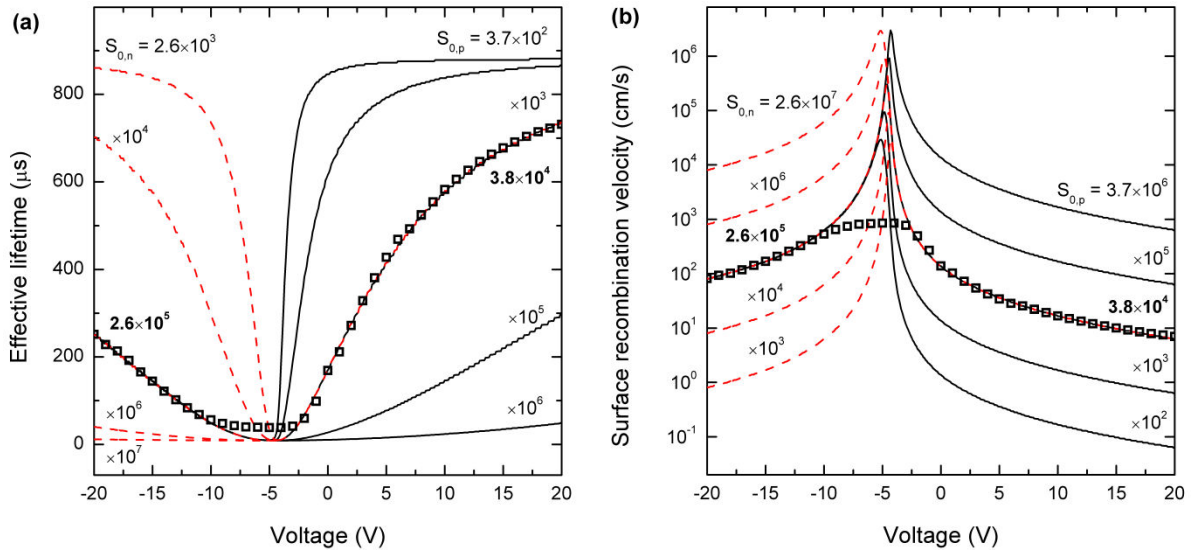


Fig. 5.

Measured (symbols) and calculated (lines) effective lifetime (a) and SRV (b) as a function of applied gate voltage for the p-type sample. Dashed lines indicate the effect of varying the $S_{0,n}$ parameter with fixed $S_{0,p} = 3.7 \cdot 10^4$ cm/s, whereas solid lines show a variation of $S_{0,p}$ with fixed $S_{0,n} = 2.6 \cdot 10^5$ cm/s. Other simulation parameters are given in Table 2.

As shown in figure 2, there is a discrepancy between the experimental data and the theoretical models in the depletion region of the curve, where τ_{eff} goes through a minimum. This is illustrated more clearly in Fig. 5(b), which shows how the modeled rear SRV of the p-type sample increases by several orders of magnitude as the curve approaches the point where $n_s \approx p_s$. In contrast, the SRV calculated from the experimental data has a maximum value at ~ 850 cm/s for the p-type sample and ~ 320 cm/s for the n-type sample. We believe that this difference indicates that the models described in section 4.1 and 4.2 do not fully describe the recombination at the a-SiN_x:H/c-Si interface under depletion conditions when the SRV is large. For instance, the Girisch model assumes constant quasi-Fermi levels of electrons and holes throughout the surface space region, which may not be the case for the largest SRVs observed at depletion conditions. Also, the Girisch model does not sufficiently describe the strong injection level dependence of the SRV that is observed in a-SiN_x:H passivated p-type wafers under low injection conditions. A more complex model including recombination at subsurface defects in the surface space charge region has been proposed to explain this behavior [4], [18]. This model has however not been implemented in this work as the simpler models has been found to describe the data sufficiently well with fewer assumptions and free parameters.

4.4. Leakage currents and charge stability

C-V measurements of MIS-structures made from PECVD a-SiN_x:H often suffer from hysteresis effects caused by injection of charge carriers from the Si substrate into a-SiN_x:H bulk traps [12]. A similar behavior may also be observed during the PL-V measurement: A constant DC voltage applied over the a-SiN_x:H layer over several seconds may cause build-up of charge in the film, leading to a permanent change in the PL signal after the voltage is removed. To avoid any large errors arising from this effect the samples were made with stoichiometric a-SiN_x:H layers with a refractive index of ~ 1.9 , where the charge buildup is less pronounced. To prevent the error from building up over time, the measurement were done at alternating voltage with increasing absolute values. A control measurement at 0 V was performed between each measurement with applied voltage in order to monitor the possible change in the measured signal. By following these precautions we found a maximum total deviation of less than 8 % in the 0 V signal, much less after measuring the data points at voltages with an absolute value < 10 V.

Leakage currents during measurements should be avoided, as these may cause unwanted voltage drops or charge carrier injection influencing the measured PL signal. The probability of producing capacitors that are leaking due to pinholes through the a-SiN_x:H layer is higher for the large PL-V electrodes than for the small pads used for C-V samples. This problem could however be circumvented by depositing a relatively thick (120 nm) layer of a-SiN_x:H. The leakage current passing through the samples was monitored during the measurements and was found to stay below 1 μ A even at the highest gate voltages.

Several electrodes for PL-V measurements was deposited on each sample. In this way we could both avoid leaking pads and get better measurement statistics. In principle, a large grid of pads may be measured at the same time, enabling fast measurements of the lateral variation of surface passivation properties. Both this feature and the ability to quantify the measurement errors from non-ideal materials like PECVD a-SiN_x:H may be important advantages of the PL-V method over alternative techniques like corona charging.

5. Conclusions

In this paper we have presented an alternative characterization technique for analyzing the surface recombination for passivated Si surfaces while precisely controlling the surface band bending. The method, which has been abbreviated PL-V, uses a photoluminescence imaging setup to measure the effective lifetime of the sample. By applying a voltage to an electrode placed on the bottom side of the structure the rear side SRV may then be varied without obstructing the light excitation or lifetime measurement itself.

To illustrate the potential of the method, PL-V measurements have been performed on both p-type and n-type Si wafers passivated by PECVD a-SiN_x:H layers. We have described how the results from these measurements may be interpreted to independently extract information about the chemical passivation, that is, the properties of the recombination-active surface defects (through $S_{0,n}$ and $S_{0,p}$) and the field effect passivation (through Q_f) of a passivated Si surface.

The ratio between electron and hole capture σ_n/σ_p at the a-SiN_x:H passivated surface was found to be ~ 7 for the p-type sample and ~ 5 for the n-type sample. In both cases, the fixed charge density Q_f under illumination was found to be $6.1 - 6.5 \cdot 10^{11}$ cm⁻², similar to the values obtained by dark C-V measurements.

Acknowledgements

This work has been funded by the Research Council of Norway through the project "Thin and highly efficient silicon-based solar cells incorporating nanostructures," NFR Project No. 181884/S1

References

- [1] E. Yablonovitch, R. M. Swanson, W. D. Eades, and B. R. Weinberger, "Electron-hole recombination at the Si-SiO₂ interface," *Applied Physics Letters*, vol. 48, no. 3, pp. 245-247, 1986.
- [2] R. B. M. Girisch, R. P. Mertens, and R. F. De Keersmaecker, "Determination of Si-SiO₂ interface recombination parameters using a gate-controlled point-junction diode under illumination," *IEEE Transactions on Electron Devices*, vol. 35, no. 2, pp. 203-222, 1988.
- [3] M. Schoffhale, R. Brendel, G. Langguth, and J. H. Werner, "High-quality surface passivation by corona-charged oxides for semiconductor surface characterization," in *Conference Record of the Twenty Fourth. IEEE Photovoltaic Specialists Conference*, 1994, vol. 2, pp. 1509-1512.
- [4] S. W. Glunz, D. Biro, S. Rein, and W. Warta, "Field-effect passivation of the SiO₂/Si interface," *Journal of Applied Physics*, vol. 86, no. 1, p. 683, 1999.
- [5] T. Trupke, R. A. Bardos, M. C. Schubert, and W. Warta, "Photoluminescence imaging of silicon wafers," *Applied Physics Letters*, vol. 89, no. 4, pp. 44103-44107, 2006.
- [6] W. Kern, "The Evolution of Silicon Wafer Cleaning Technology," *Journal of The Electrochemical Society*, vol. 137, no. 6, pp. 1887-1892, 1990.
- [7] S. Herlufsen, J. Schmidt, D. Hinken, K. Bothe, and R. Brendel, "Camera-based photoluminescence imaging of crystalline silicon wafers," in *24th European Photovoltaic Solar Energy Conference*, 2009, pp. 913-917.
- [8] H. Nagel, C. Berge, and A. G. Aberle, "Generalized analysis of quasi-steady-state and quasi-transient measurements of carrier lifetimes in semiconductors," *Journal of Applied Physics*, vol. 86, no. 11, pp. 6218-6221, 1999.
- [9] E. . Nicollian and J. R. Brews, *MOS (metal oxide semiconductor) physics and technology*. John Wiley & Sons, Inc., 2003.
- [10] S. De Wolf, G. Agostinelli, G. Beaucarne, and P. Vitanov, "Influence of stoichiometry of direct plasma-enhanced chemical vapor deposited SiN_x films and silicon substrate surface roughness on surface passivation," *Journal of Applied Physics*, vol. 97, no. 6, pp. 63303-63308, 2005.
- [11] J. F. Lelièvre, E. Fourmond, A. Kaminski, O. Palais, D. Ballutaud, and M. Lemiti, "Study of the composition of hydrogenated silicon nitride SiN_x:H for efficient surface and bulk passivation of silicon," *Solar Energy Materials and Solar Cells*, vol. 93, no. 8, pp. 1281-1289, 2009.
- [12] J. Schmidt and A. G. Aberle, "Carrier recombination at silicon-silicon nitride interfaces fabricated by plasma-enhanced chemical vapor deposition," *Journal of Applied Physics*, vol. 85, no. 7, pp. 3626-3633, 1999.
- [13] A. G. Aberle, S. Glunz, and W. Warta, "Impact of illumination level and oxide parameters on Shockley-Read-Hall recombination at the Si-SiO₂ interface," *Journal of Applied Physics*, vol. 71, no. 9, pp. 4422-4431, 1992.
- [14] W. Eades and R. Swanson, "Calculation of surface generation and recombination velocities at the Si-SiO₂ interface," *Journal of Applied Physics*, vol. 58, no. 11, p. 4267, 1985.
- [15] A. B. Sproul, "Dimensionless solution of the equation describing the effect of surface recombination on carrier decay in semiconductors," *Journal of Applied Physics*, vol. 76, no. 5, pp. 2851-2854, 1994.
- [16] P. A. Basore and D. A. Clugston, "PC1D Version 4 for Windows: From Analysis to Design," in *25th IEEE Photovoltaic Specialists Conference, Washington*, 1996, pp. 377-381.
- [17] S. Dauwe, J. Schmidt, A. Metz, and R. Hezel, "Fixed charge density in silicon nitride films on crystalline silicon surfaces under illumination," *Conference Record of the Twenty-Ninth IEEE Photovoltaic Specialists Conference, 2002.*, pp. 162-165.
- [18] S. Steingrube, P. P. Altermatt, D. S. Steingrube, J. Schmidt, and R. Brendel, "Interpretation of recombination at c-Si/SiN_x interfaces by surface damage," *Journal of Applied Physics*, vol. 108, no. 1, p. 014506, 2010.